Journal of the Korean Chemical Society
2022, *Vol. 66, No. 5*
Printed in the Republic of Korea
https://doi.org/10.5012/jkcs.2022.66.5.349

Advances of Isomerizing-hydrogenating Properties of CoMo Catalysts Supported on ASA-Al_2O_3

E. A. Avdeenko*, K. A. Nadeina, T. V. Larina, V. P. Pakharukova, E. Yu. Gerasimov, I. P. Prosvirin, A. A. Gabrienko, Yu. V. Vatutina, O. V. Klimov, and A. S. Noskov

Boreskov Institute of Catalysis SB RAS, Lavrentiev pr. 5, Novosibirsk, Russia, 630090
**E-mail: sea@catalysis.ru*

(Received May 6, 2022; Accepted July 23, 2022)

ABSTRACT. Because hydrotreating (HDT) of FCC gasoline is one of the important processes used to prepare such gasoline for blending, the development of a catalyst for this process is of great interest. Currently, the industrial HDT of FCC gasoline consists of two stages and the creation of a new catalyst for one-stage HDT will make this process more efficient. Recently, our group has developed the CoMo/Al_2O_3-ASA catalyst and studied the influence of Si/Al ratio on the target reactions of HDT process. Despite the high selectivity and activity, the catalyst with ASA is not applicable in industry because of its low strength. The present work moves forward to study the influence of the ASA content in the catalyst support and clarify the possibility to develop the catalyst that combines high activity and selectivity in HDT reactions with successful performance. Here we show that the CoMo catalyst with ASA/Al_2O_3 molar ratio 1/1 in the support is the best combination for FCC gasoline hydrotreatment due to exceptional properties of the catalyst composition.

Key words: FCC gasoline, Hydrotreating catalyst, Selective hydrodesulphurization, Aluminosilicate, Octane number

INTRODUCTION

Hydrotreating is one of the most large-scale oil refining processes.[1,2] The predecessors of modern hydrotreating catalysts were bulk catalysts based on various sulfides. Numerous researches showed that the combination of molybdenum/tungsten sulfides doped by cobalt/nickel has the high activity in hydrotreating reactions.[3,4] It was later discovered that the highest activity in hydrotreating process was achieved when the CoMoS or NiMoS phase was formed on the catalyst surface.[5,6]

Currently, the vast majority of hydroprocessing catalysts consist of the sulfide active phase supported on a porous carrier.[7–9] Gamma-aluminum oxide is usually used as a support due to its almost complete inertness to reactions occurring in the process, relatively low cost and the ability to adjust its textural and strength characteristics.[10–12] However, quite a lot of attention has recently been paid to the search for alternative supports capable of increasing the activity of catalysts due to their own properties. Thus, the addition of Si-containing components, such as amorphous aluminosilicates[13,14] or zeolites,[15,16] to alumina support is quite common.

Amorphous aluminosilicates (ASA) are becoming widely used due to the presence of a certain set of acid sites that can catalyze various reactions, and also due to their relatively low cost. For example, it is shown in[13,17–19] that ASA could promote isomerization and aromatization reactions. The use of ASA in hydrotreating catalysts allows the improvement of catalytic activity in hydrodesulfurization and hydrodenitrogenation reactions.[20–22]

The increased ability of hydrotreating catalysts to isomerization reactions is a distinct advantage in a process such as catalytic cracking gasoline hydrotreatment. It was recently found that isomerization activity of aluminosilicate component to olefins provides conversion of low-octane component to its high-octane derivative, as well as the reduction in contribution to hydrogenation reaction of olefin.[17–19] These effects make it possible to preserve the octane number of the product, which is one of the most important indicators for this type of catalyst. At the same time, high activity in the conversion of sulfur-containing components is achieved due to the presence of the CoMoS phase in such catalysts. This makes it possible to obtain high-octane ultra-clean fuel.

Previously, our group investigated the variation of the Si/Al ratio in ASA and the effect on the activity and selectivity of ASA-containing catalysts in hydrotreating of FCC gasoline.[13] It has been established that the CoMo catalyst containing ASA with the ratio Si/Al = 0.25 has the best properties. However, ASA-containing catalysts are forced to contain composite supports consisting of ASA

and Al_2O_3 components. This is because the ASA powder itself cannot be molded even with the use of a plasticizer. Therefore, the introduction of an alumina precursor during molding is a required parameter of the synthesis. Despite the fact that the ASA component of the support is very important, the properties of the alumina component must be taken into account since it in fact determines the kneading properties of the paste and the strength characteristics of the support and catalyst. The main question in this case is how much alumina can be incorporated in order to create a sufficiently strong catalyst without losing the activity advantage.

The present work studies the effect of the Al_2O_3/ASA ratio in the composition of the support in CoMo/Al_2O_3-ASA hydrotreating catalyst in order to find the key parameters that are required to achieve high activity and selectivity of the catalyst in the conversion of FCC gasoline while obtaining good performance.

EXPERIMENTAL

Preparation of ASA, Pseudoboehmite, Support and Catalyst

An amorphous aluminosilicate (ASA) powder was prepared by the coprecipitation method described in.[13] The aluminum sulfate and sodium silicate solutions were used as aluminum and silicon precursors. The Si/Al mass ratio in ASA was 0.25. A pseudoboehmite (PBe) powder was prepared by hydrothermal treatment of CTA product as described in.[23]

The ASA and PBe powders were used to prepare supports with different Al_2O_3/ASA weight ratios: 100/0, 90/10, 70/30, 50/50, 30/70, 10/90, and 0/100. The supports were designated as Sup-(ratio). An aqueous solution of nitric acid was used for peptization. The HNO_3/Al_2O_3 molar ratio was 0.03 for supports with 50–100 wt.% Al_2O_3. When Al_2O_3 content was less than 50 wt.%, the HNO_3/Al_2O_3 molar ratio was 0.06–0.15 in order to achieve plasticity and formability of a kneading paste. Preliminary dry mixing of the PBe and ASA powders took place. After that, an aqueous solution of a peptizing agent was added to the mixture of dry components, and stirring continued until a plastic mass was obtained. Kneading pastes were extruded using a fluoroplastic spinneret with trilobe holes. The diameter of circumscribe circle of the support granules in all cases was 1.5 mm. Granulated supports were dried at 110℃ for 2 hours and calcined at 550℃ for 4 hours in an air flow.

CoMo/Al_2O_3-ASA catalysts were prepared by wetness impregnation technique. The impregnating solution was synthesized by sequential dissolution of citric acid monohydrate $C_6H_8O_7 \cdot H_2O$, ammonium heptamolybdate tetrahydrate $(NH_4)_6Mo_7O_{24} \cdot 4H_2O$ and cobalt hydroxide $Co(OH)_2$ at 50℃. Concentrations of reagents were chosen to obtain 6.0±0.2 wt.% Mo and 2.0±0.1 wt.% Co in the final catalysts. Molar ratio of Co/citric acid was 1:1.1. The wetness impregnation was carried out with slow rotation for 60 minutes at a temperature of 50℃. Catalysts were dried at 120℃ for 2 hours followed by calcination at 550℃ for 4 hours in an air flow. Calcined catalysts were crushed by hand to obtain a fraction of 0.5–0.25 mm.

Catalytic Tests

The catalyst fraction was sulfided in a H_2S flow (500 h^{-1}) at atmospheric pressure. Sulfidation was performed in two stages – 2 h at 200℃ and 2 h at 400℃. The H_2S flow was in exceed to the content of active metals in the catalysts. To avoid oxidation, the catalysts were cooled and stored in a He flow before catalytic tests.

Catalytic tests of hydrotreating of a model feedstock were carried out in a fixed bed reactor. Sulfided catalyst fraction (1 cm^3) was uniformly mixed with SiC fraction (1 cm^3) and placed in the isothermal zone of the reactor. The model feedstock contained 40 wt.% toluene, 40 wt.% cyclohexane, and 20 wt.% 1-hexene. Thiophene was used as a sulfur-containing compound (250 ppm S). The testing conditions were as follows: P = 2.5 MPa, LHSV = 10.0 h^{-1}, H_2/feed ratio = 200 nm^3/m^3, T = 220 and 240℃. Catalysts were previously handled in the feedstock flow at 200℃ for 24 h at the beginning of the test. Then, the temperature was raised to 220℃. Upon reaching the operating temperature, the catalyst was running for 12 hours without sampling. Then, 3 liquid and 2 gas samples were taken for each regime.

Composition of the model feedstock, gas and liquid products was analyzed using an Arnel 4050 Clarus (PerkinElmer, United States) chromatograph analyzer equipped with a capillary column Rtx-DHA (100 m, 0.25 mm ID, 0.5 μm). Sulfur content in the model feedstock and liquid products was determined with an XPLORER TN/TS (TE Instruments, Netherlands) according to ASTM 5453. Density measurements of the liquid products and model mixture were carried out using a Densito 30PX Portable Density Meter (METTLER TOLEDO, United States) according to ASTM D 7777.

Characterization

Chemical composition of samples was determined by inductively coupled plasma atomic-emission spectros-

copy on an Optima 4300 DV spectrometer (PerkinElmer, United States).

Textural properties of the catalysts, supports, ASA and PBe were determined by nitrogen physisorption using an ASAP 2400 (USA) instrument as described in.[24] Prior to the analysis, samples were heated in a N_2 flow at 200℃ for 2 h.

Thermoprogrammed desorption of ammonia (NH_3 TPD) was made on a ChemBET Pulsar TPR/TPD instrument (Quantachrome Instruments, United States) equipped with a thermal conductivity detector. 100 mg of a sample (the 0.25–0.50 mm fraction) were loaded to a quartz U-shaped tube. The position of the sample in the tube was fixed with quartz wool. The sample was blown with a 20 cm^3/min He flow while heating to 550℃ with a rate of 20℃/min and kept at this temperature for 30 min to remove moisture. Then, the temperature was lowered to 100℃ and a blank experiment was carried out. For this, the sample was heated to 550℃ with a rate of 10℃/min in the 20 cm^3/min He flow and kept at this temperature for 30 min. Then the sample was cooled to 100℃ and purged with ammonia for 15 min with a rate of 20 cm^3/min. The sample was purged with the 20 cm^3/min helium flow at 100℃ for 30 min in order to remove physisorbed ammonia. For NH_3 TPD, the sample was heated to 550℃ with a rate of 10℃/min in the 20 cm^3/min helium flow and kept at this temperature for 30 min. The amount of desorbed ammonia was calculated by integrating the signal area and using instrument calibration with a standard ammonia amount.

IR spectroscopy of adsorbed pyridine (Py-IR) was carried out on a Varian Scimitar 1000 FTIR spectrometer equipped with a high-temperature flow cell with CaF_2 windows. FTIR measurements were performed on self-supported wafers with a density of 15 mg/cm^2 and activated in a vacuum at 150℃. Pyridine adsorption was carried out by dropwise injections of purified pyridine (up to 10 lL) using a microliter syringe into the gas line through a septum injection port at 150℃ followed by desorption of the pyridine in a vacuum at 150, 250, 350 and 450℃. The relative amount of Brønsted acid sites (BAS) was estimated from the squares of corresponding signals in IR spectra in the range of 1400–1600 cm^{-1} using the integrated molar absorption coefficients reported by Emeis.[25]

HRTEM images were obtained on a JEM-2010 electron microscope (JEOL, Japan) with a lattice-fringe resolution of 0.14 nm at an accelerating voltage of 200. Local energy-dispersive X-ray analysis (EDXA) was carried out on an EDAX spectrometer (EDAX Co.) fitted with a Si (Li) detector with a resolution of 130 eV. The size of MoS_2 particles and the average number of layers in the package were determined using four different fragments of the sample under study, a total number of characterized particles being equal to 500.

NMR spectra were recorded on a Bruker Avance-400 spectrometer equipped with a broad-band double-resonance MAS probe (4 mm). The samples were saturated with water vapor for 20 h prior to NMR measurements. Afterwards, the powder was placed into a MAS NMR zirconia 4 mm rotor. ^{29}Si MAS NMR spectra were recorded at the resonance frequency of 79.49 MHz while the samples were spun at 8 kHz with dry compressed air. The excitation pulse ($\pi/2$) length was 7.0 μs, and 1320 scans were accumulated for a spectrum with a 60 s delay between the scans. For ^{27}Al MAS NMR spectra recorded at 104.31 MHz, the spinning rate was equal to 12–14 kHz. The total number of scans was 2000 with a repetition delay of 0.5 s, and a 0.8 μs pulse ($\pi/12$) was used. ^{29}Si and ^{27}Al chemical shifts were determined with an accuracy of ±0.1 ppm using TMS and a 0.1 M aqueous solution of $Al(NO_3)_3$ as external standards.

The optical properties of the materials were studied by diffuse reflectance electron spectroscopy using a Shimadzu UV-2501 PC spectrophotometer with an ISR-240 A diffuse reflectance attachment. Samples (the fraction < 0.25 mm) were placed in a quartz cuvette with a 2 mm optical path length. The spectra were recorded using the $BaSO_4$ reflectance standard in the range of 190-900 nm (11000-54000 cm^{-1}) with a 2 nm step. Reflection coefficients were converted using the Kubelka-Munk function $F(R) = (1 - R)^2/2R$, where R is the diffuse reflection coefficient depending on the wavenumber (cm^{-1}). The data obtained are given in the coordinates: Kubelka-Munk function F(R) – wavenumber.

X-ray photoelectron spectra (XPS) were recorded using a SPECS spectrometer with a PHOIBOS-150 hemispherical energy analyzer and $Al_{K\alpha}$ radiation ($h\nu$ = 1486.6 eV, 200 W). The binding energy scale was preliminarily calibrated against the position of $Au_{4f7/2}$ (84.0 eV) and $Cu_{2p3/2}$ (932.67 eV) core level peaks. For spectra recording, the samples were deposited on a conductive scotch tape. The method of internal standard was used for correct calibration of photoelectron peaks. The peak of C_{1s} with E_b = 284.8 eV was used.

Precalcined initial powders of PBe and ASA were studied by laser diffraction on a SALD 2101 instrument (Shimadzu Corp., Japan) (the measurement range of 0.03–1000 μm). The previously prepared suspension of a sample was subjected to ultrasonic treatment and stirred inten-

sively for 5 minutes before being placed in the measuring cell. The measurement method conforms to ASTM D 4464-15.

Powder diffraction patterns were obtained on a Bruker D8 Advance instrument (Bruker, Germany) using $Cu_{K\alpha}$ radiation ($\lambda = 1.5418$ Å) and Bragg-Brentano focusing geometry. A one-dimensional LynxEye detector with an angular range of 2.9° on the 2θ scale was used for signal recording. Measurements were performed by scanning in the range of angles 10–70° with a step of 0.05° on the 2θ scale and with 3 s accumulation time.

The bulk crushing strength (BCS) was measured by means of SMS 1471 or a similar ASTM method 7084-04 using a bulk crushing strength instrument (VINCI Technologies, France).

Calculation of Catalytic Activity

Catalytic activity in HDS reactions has been estimated as thiophene conversion (Conv(S)) according to equation (1):

$$Conv(S) = \left(1 - \frac{C_s'}{C_s}\right) \times 100\% \quad (1)$$

where C_s' is the sulfur content in the liquid product; C_s is the sulfur content in the feedstock.

Conversion of 1-hexene (designated as Conv(1-hexene)) was calculated according to Eq. (2):

$$Conv(1-hexene) = (1 - \frac{C_{1-hexene}'}{C_{1-hexene}}) \times 100\%, \quad (2)$$

where $C'_{1\text{-}hexene}$ is the summary content of 1-hexene in the liquid and gas products; $C_{1\text{-}hexene}$ is the content of 1-hexene in the initial model feedstock.

Catalysts' activities in hydrogenation reactions (designated as $HYD_{1\text{-}hexene}$) were calculated according to Eq. (3):

$$HYD_{hexene-1} = \frac{\omega'_{n-hexane}}{\omega'_{1-hexene} + \omega'_{n-hexane} + \sum \omega'_{i-hexene}} \times 100\%, \quad (3)$$

where $\omega'_{n\text{-}hexane}$ is the content of n-hexane in the liquid and gas products; $\omega'_{1\text{-}hexene}$ is the content of 1-hexene in the liquid and gas products; and $\Sigma\omega'_{i\text{-}hexene}$ is the total content of 1-hexene isomers in the liquid and gas products.

The isomerizing activity (designated as ISO) was calculated according to Eq. (4):

$$ISO = \frac{\sum \omega'_{i-hexene}}{\omega'_{1-hexene} + \omega'_{n-hexane} + \sum \omega'_{i-hexene}} \times 100\% \quad (4)$$

RON values were calculated according to Eq. (5):

$$RON = \sum_i \omega_i \times RON_i, \quad (5)$$

where ω_i is weight portions of each component in the feedstock or liquid product; RON_i is a research octane number of each component. The *RON* values of each component in the feedstock and liquid products were taken from data in.[26]

RESULTS AND DISCUSSION

Chemical compositions of the synthesized supports and catalysts are given in *Table* 1. The data of ICP-AES analysis fit in well with theoretical calculations. Si, Al, Mo and Co contents coincide with expected values. An increase in Al_2O_3/ASA ratio in the support also increases its water capacity from 0.5 to 2.8 cm^3/g. Such great values could be useful in the case when solutions with high concentration of active metals are used. In our case, the water capacity values are much higher than needed.

The ASA powder itself has very poor plasticizing ability. If aqueous solution of nitric acid is added to the ASA powder, the granulated support will have a bulk crushing strength value less than 0.3 MPa because of bad properties of the kneading paste. The addition of 30–50 wt.% aluminum hydroxide to the kneading paste increases the BCS value up to 0.4 MPa. Greater amounts of PBe (more

***Table* 1.** Chemical composition and physical parameters of supports and catalysts

Supports						Catalysts			
Al_2O_3/ASA ratio	Si, wt.%	Al, wt.%	BCS, MPa	Water capacity, cm^3/g	Bulk density, g/cm^3	Co, wt.%	Mo, wt.%	BCS, MPa	Bulk density, g/cm^3
100/0	-	52.9	1.4	0.5	0.7	2.1	6.1	1.6	0.8
90/10	1.1	51.8	1.2	0.6	0.6	2.1	6.1	1.4	0.7
70/30	2.9	49.7	0.8	1.0	0.5	2.1	6.0	0.9	0.5
50/50	4.8	47.8	0.5	1.7	0.3	2.0	6.1	0.7	0.4
30/70	6.7	46.0	0.4	2.0	0.3	2.1	6.1	0.6	0.3
10/90	8.6	43.6	<0.3	2.8	0.2	2.1	6.0	0.35	0.3
0/100	9.9	41.8	<0.3	2.5	0.2	2.1	6.1	<0.3	0.2

than 90 wt.%) provide strong supports with BCS values above 1.2 MPa. Small quantities of active metals do not provide high BSC values for the catalysts with less than 90 wt.% of alumina, but the catalysts with 30–50 wt.% in a granular shape are strong enough to endure storage and overloading from one container to another.

The synthesis of the composite support requires studies of its phase composition. After thermal treatment at 550℃, aluminosilicate did not transform to another phase, as it was evidenced by the ^{29}Si MAS NMR spectrum of Sup-0/100 (*Fig.* SI1). Deconvolution of the Sup-0/100 spectrum reveals the presence of five overlapping signals in the region from –70 to –110 ppm. These signals can be assigned to tetrahedrally bonded silicon atoms neighbored by a varying number of aluminum atoms, i.e. Q4(nAl) units where n = 0÷4.[27] The integral intensities of the observed signals were used to calculate Si/Al ratio of 2.0 for the Sup-0/100 sample.

^{27}Al MAS NMR spectroscopy enables one to distinguish reliably aluminum atoms with different coordination numbers, which are present in aluminosilicate materials.[27] The Sup-0/100 support (100% ASA) contains three types of Al atoms located in AlO_4, AlO_5 and AlO_6 units with the relative intensities of 26, 15, and 59%, respectively (*Fig.* SI2). The spectrum of the Sup-100/0 sample (pure γ-Al_2O_3) reveals two signals corresponding to tetrahedrally and octahedrally coordinated Al atoms. The AlO_4/AlO_6 ratio is 0.5 (*Fig.* SI2). The ^{27}Al MAS NMR spectrum of the Sup-50/50 sample (*Fig.* SI2) is a superposition of the spectra of its constituents. All three types of AlO_m units (m = 4, 5, 6) are present in the spectrum. The relative content of different Al atoms is 31, 8 and 61% for four-, five-, and six-fold coordinated aluminum, respectively.

To understand the state of Al_2O_3, the supports were studied by XRD (*Fig.* SI3). The diffraction pattern of the Sup-100/0 sample corresponds to a metastable low-temperature phase of γ-Al_2O_3 with the spinel cubic structure (PDF#00-029-0063). Parameters of the crystal lattice are a = b = c = 7.907(2) Å, the average size of CSR is D = 5.5 nm. The diffraction pattern of the Sup-0/100 sample does not contain clear maxima because of the X-ray amorphous properties. The broadened peak at 2θ = 65.5° cannot be ascribed to a poorly crystallized phase of alumina because it is shifted to smaller angles. Diffraction patterns of the samples with different Al_2O_3/ASA ratio show an increased contribution of metastable γ-Al_2O_3 in the samples with high alumina content.

Based on the data obtained, it can be concluded that the supports with Si/Al ratio 90/10, 70/30, 50/50, 30/70 and 10/90 are the mixture of ASA and Al_2O_3 and do not include other phases.

If we have two separate phases in supports, it can be suggested that textural properties will be a superposition of the texture of individual components. Indeed, specific surface area of the supports increases with an increase in their ASA content. It is noted that the most drastic increase is observed when the ASA content grows from 0 to 50% (*Fig.* 1(A)). Further increase in the content of ASA does not lead to such strong changes. The same tendency is observed for pore volume values of the supports (*Table* SI4).

Because the catalysts contained low amounts of active metals and further testing of the catalysts included only testing in the model feedstock, such high SSA values and great pore volume are more than enough for great diffusion of the feedstock molecules through pores of the catalysts. However, we considered changes in pore size distribution of the supports with changes of ASA content (*Fig.* 1B). It was not expected that a gradual increase in ASA content would change the pore size distribution in a strange manner. When ASA content becomes higher, the portion of pores with diameters < 50 Å and 50-100 Å becomes lower. The portion of pores with diameters > 200 Å

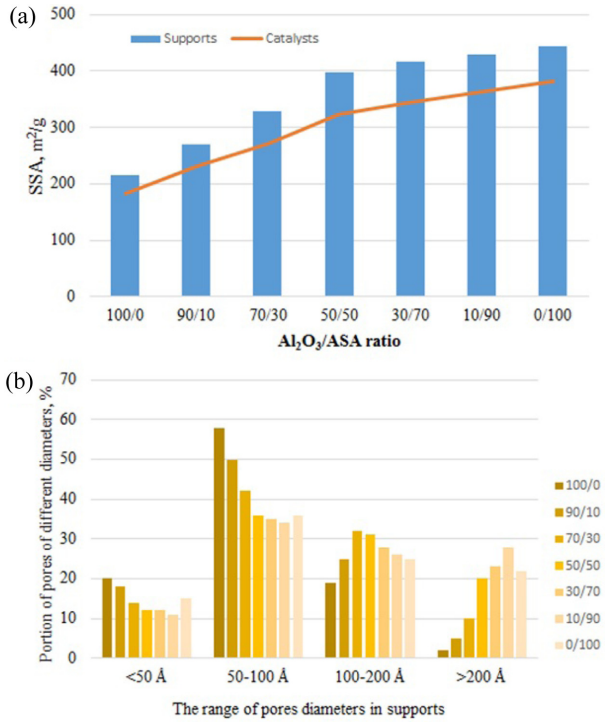

***Figure* 1.** Specific surface area of supports and catalysts (a) and pore portion of different diameters in supports (b).

increases with the amount of ASA. The changes concerning pores with diameters 100-200 Å show a volcanic dependence. The greatest amount of such pores is observed for the Sup-70/30 and Sup-50/50 samples.

After supporting active metals, the SSA and pore volume values become lower; however, the textural properties change in a similar manner with the ASA content in the corresponding supports.

A quick glance at the pore size distribution curves of supports and catalysts (*Fig*. SI5) confirms the wide pore size distribution for the ASA-containing supports. The amount of wide pores becomes greater with the ASA content, but the addition of ASA also contributes to small pores (with diameters < 40 Å).

Most attractive in the introduction of ASA into support are changes in the support acidity. If we talk about isomerization and hydrogenation reactions, the most pronounced effects will be obtained for catalysts prepared from the supports with higher acidity than alumina. According to TPD-NH_3 data, the total concentration of acid sites of the parent Al_2O_3 sample is by 40% lower than that of the ASA powder (*Table* 2). Indeed, the initial Al_2O_3 contains a much lower amount of weak and medium acid sites, while the amount of strong acid sites is similar.

The amount of acid sites of different strength in supports is not an algebraic sum of their components multiplied by the content of each component. The concentration of weak acid sites significantly increases after peptization of supports by nitric acid. There is no clear tendency in the change of the concentration of medium and strong acid sites. It was also noted that the addition of 10–50% of ASA into the support led to a decrease in the concentration of acid sites per m^2 of a sample from 2.0 to 1.2 (*Table* 2). Further increase in the ASA content to 100% resulted in a slight increase in this parameter to 1.5. This tendency is not observed for the catalysts that show a gradual decrease in acidity with the ASA addition. Changes in the concentration of acid sites per m^2 of a support, as will be seen below, correlate with changes in hydrogenation and isomerization activities of the catalysts.

The TPD-NH_3 method cannot identify LAS and BAS. So we used the IR of pyridine adsorption to measure the concentration of BAS sites (*Table* 3). ASA in the supports contribute to the formation of BAS. The formation of weak acid sites is observed for the supports with ASA. Moreover, an increase in the ASA content from 50 to 100% doubles the amount of Brønsted acid sites in the supports. It is noted that the total amount of BAS sites is not much higher than the amount of weak sites. Then, the contribution of medium and strong BAS is not significant. Besides, the

***Table* 3.** Acidity data obtained by IR of pyridine adsorption

Al_2O_3/ASA ratio	Sample	Brønsted acid sites, μmol/g	
		Weak	Total
100/0	Support	0	0
	Catalyst	0	0
50/50	Support	11	15
	Catalyst	14	18
0/100	Support	21	25
	Catalyst	25	29

***Table* 2.** NH_3-TPD data

Al_2O_3/ASA ratio	Sample	Concentration of acid sites, μmol/g				Concentration of acid sites per 1 m^2 of the sample
		Weak	Medium	Strong	Total	
Parent ASA		183	362	76	621	1.3
PBe calcined at 550℃		92	237	54	384	1.7
100/0	Sup	113	251	72	432	2.0
	Cat	138	258	93	489	2.7
90/10	Sup	122	257	61	440	1.6
	Cat	154	276	81	505	2.2
70/30	Sup	137	271	54	462	1.4
	Cat	173	315	83	571	2.1
50/50	Sup	160	280	47	488	1.2
	Cat	179	370	87	636	2.0
30/70	Sup	170	355	84	608	1.5
	Cat	203	389	86	678	2.0
10/90	Sup	174	369	70	613	1.4
	Cat	225	383	74	682	1.9
0/100	Sup	201	390	73	664	1.5
	Cat	219	416	69	704	1.8

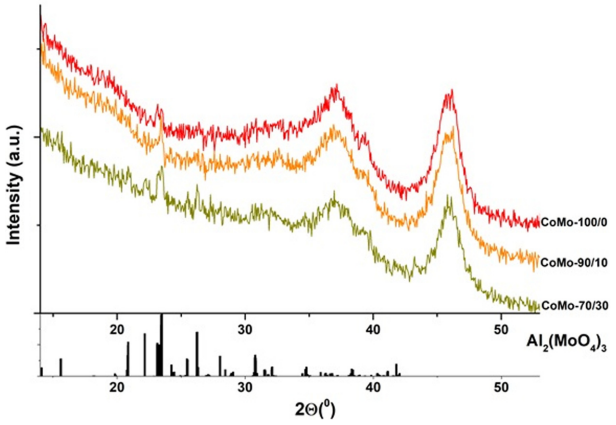

***Figure* 2.** X-ray diffraction patterns of the catalysts with 100–70 wt.% of alumina in the support.

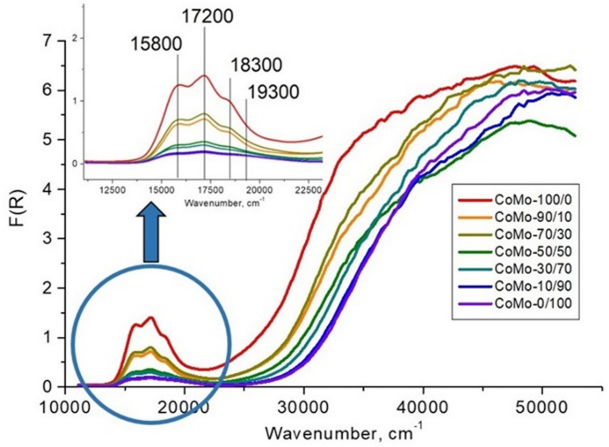

***Figure* 3.** DRS spectra of calcined CoMo/Al_2O_3-ASA catalysts.

observed gradual increase in the amount of BAS of different strength allows us to conclude that the uneven change in strong acid sites seen in TPD-NH_3 data is caused by strong LAS sites.

The addition of ASA to the support and catalyst is expected to change the interaction between active metals and a support. The XRD data of catalysts show no structural changes of the supports after supporting active metals. XRD patterns of the catalysts with 100–70 wt.% of alumina in the support contain additional narrow peaks with a low intensity at $2\theta = 20.8$, 22.1, 23.4 and 26.3° (*Fig.* 2), which correspond to the $Al_2(MoO_4)_3$ phase (PDF#00-023-0764). The formation of $Al_2(MoO_4)_3$ is not observed for the samples with the ASA content higher than 50 wt.%. Therefore, the interaction between active metals and a support weakens when ASA content in the support exceeds 70%. Then, changes in the oxidation state of active metals can occur.

The oxidation state and coordination numbers of Co and Mo cations were determined from the absorption spectrum obtained by DRS (*Fig.* 3). The energy values of the adsorption bands of Co and Mo cations were related to the values of d-d transitions common for Me cations. In all cases, the spectra could be divided into three areas: the area from 13000 to 22000–23000 cm^{-1}, the area at 22000–23000 cm^{-1} with high intensity, and the area from 11000 to 13000 cm^{-1} with the lowest intensity.

It is established that intensity of the bands in the range of 11000–13000 cm^{-1} grows with ASA content in the supports, which is caused by the presence of trace components in the initial ASA powder. According to chemical analysis data of the supports, the ASA powder contains about 0.08 wt.% of Na and 0.05 wt.% of Fe.

Adsorption bands in the range of 13000 to 22000–23000 cm^{-1} are characteristic for Co^{2+} cations in the tetrahedral Co^{2+}_{Td} and octahedral Co^{2+}_{Oh} oxygen surrounding. Shifts of adsorption bands for all the cations significantly depend on the strength of crystalline field formed by ligands of the first and second coordination spheres. For all the studied catalysts, three bands at 15800, 17200 and 18300 cm^{-1} appear in this range. These bands correspond to Co^{2+}_{Td} stabilized in $CoAl_2O_4$. It is caused by the d-d transition of $^4A_2(F)$–$^4T_1(P)$. In this case, the spinel can be reversed by 20% and also contains Co^{2+}_{Oh} cations, which appear as a low-intensity band with the position of 21000 cm^{-1}. An increase in the ASA content in supports results in a gradual drop in intensity of the bands at 15800, 17200 and 18300 cm^{-1}, which indicates a decrease in the amount of Co^{2+}_{Td} cations and formation of Co^{2+}_{Oh}. In addition, adsorption bands in the range of 20000 cm^{-1} appear for the samples with more than 30 wt.% of ASA in the support. Most likely, these bands correspond to the formation of Co^{2+}_{Oh} stabilized in the ASA layers. Broadening of the band maximum at 18000 cm^{-1} and its slight shift to 19300 cm^{-1} are clearly seen for the samples with 90% and 10% ASA in the support. Such band is common for stabilization of Co^{2+}_{Oh} cations in zeolites.

In the UV area of DRS spectra, there are only bands from the charge transition between metal and ligand (CTML) for the metal's cation. The CTML can appear for both the Co^{2+} and Mo^{6+} cations in the range of 22000–23000 cm^{-1}. Since CTMLs for Co^{2+}_{Td} and Co^{2+}_{Oh} are higher than 40000 cm^{-1},[28] it can be assumed that there is only the CTML from Mo^{6+} in the range of 22000–40000 cm^{-1} in the studied samples. An increase in the ASA content in supports results in a decrease in the CTML intensity from Mo^{6+} and its

shift to UV range of the spectra. Thus, there is the blue shift that can indicate a decrease in the particle size of the active component precursors.

In the present work, the oxide state of CoMo catalysts is a precursor of the sulfide active component. Obviously, the weakening interaction between the oxide precursor and support should alter the morphology of sulfide active component particles.

Examples of HRTEM images of ASA and alumina fragments of the CoMo-50/50 catalyst are shown in *Fig*. SI6. Noteworthy are the remarkable differences in location of the active component particles on alumina and ASA surfaces (*Table* 4). CoMoS particles on the alumina surface have higher stacking numbers, higher amount of slabs per surface unit and shorter particles compared to those over the ASA surface. About 40% of all CoMoS phase slabs on alumina have a multilayered structure (*Table* 4). The ASA surface preferentially contains long monolayer particles with the average length of 2.8–3.0 nm and the average stacking number of 1.6–1.7.

The morphology of the active component particles over ASA and Al_2O_3 constituents of supports contradicts the literature data. It is often observed that the stacking of the crystallites is enhanced when silica is incorporated into alumina support, while the particle length is similar or shorter.[29,30] However, the data in[30] also show that the promotion of the W/SiO_2-Al_2O_3 catalyst by Ni leads to a decrease in the particle length and stacking of the sulfide active component. Then, we can suggest a similar effect for our catalysts: the weakening interaction between active metals and support (especially detected by XRD and UV methods for Co) could result in the lowering stacking number in CoMo catalysts doped by ASA due to the improved promotion of sulfide active component.

Mo_{3d}, Co_{2p}, S_{2s}, S_{2p}, Al_{KLL} and Si_{2p} XPS spectra of sulfide CoMo catalysts are shown in *Fig.* SI7. The XPS spectra of Si and Al contain a wide peak at 102.5–102.7 eV, which corresponds to Si in the oxygen surrounding. Different Si and O bonding and possible formation of Si-O-Al bonds account for a great width of the peak. It is consistent with the ^{29}Si NMR data. The decreasing ASA content results in a decrease in the intensity of the peak.

Mo_{3d} spectra show that the ASA content in supports has a significant impact on the Mo state. The peak at 228.9 eV is characteristic for Mo^{4+} ions in the sulfur surrounding (*Fig.* SI7) in the composition of CoMoS phase.[13,31,32] Deconvolution of the peak into individual components shows the presence of Mo in the form of Mo^{5+} and Mo^{6+} (*Fig.* SI8). Concentrations of various molybdenum states in sulfide catalysts are given in *Table* 5. There is a gradual reduction in the Mo^{4+} content and an increase in Mo^{5+} with increasing ASA content in supports, while the portion of Mo^{6+} is similar (8–10%). It was noted that the Mo/S ratio on the surface increased when more than 30% of ASA was added to the support.

Co_{2p} spectra of the catalysts contain a peak with the binding energy 779.0 eV. It corresponds to cobalt II in the sulfur-oxygen surrounding.[33] The presence of a peak at 162.0 ± 0.2 eV, which is common for S^{2-} ions, and a peak at 779.0 eV in Co_{2p} spectra indicates the formation of the CoMoS phase in sulfide catalysts.[34,35] It was impossible to make deconvolution of Co_{2p} spectra because of their low

***Table* 4.** HRTEM data for CoMo sulfide catalysts

Sample	Location of active component	Average slabs number per 1000 nm^2	Average stacking number	Average slab length, nm	Portion of active component particles with different stacking numbers,%			
					1 layer	2 layers	3 layers	4+ layers
CoMo-100/0	Al_2O_3	33	2.2	2.2	35	30	25	10
	ASA	–	–	–	–	–	–	–
CoMo-90/10	Al_2O_3	27	2.3	2.3	27	33	29	11
	ASA	12	1.6	2.8	54	31	12	3
CoMo-70/30	Al_2O_3	26	2.3	2.3	25	35	30	10
	ASA	13	1.6	2.9	54	32	11	3
CoMo-50/50	Al_2O_3	25	2.3	2.4	22	34	33	11
	ASA	14	1.7	2.8	50	33	14	3
CoMo-30/70	Al_2O_3	26	2.3	2.3	24	37	29	10
	ASA	14	1.7	2.9	49	35	12	4
CoMo-10/90	Al_2O_3	27	2.4	2.3	24	38	28	10
	ASA	13	1.6	3	52	33	12	3
CoMo-0/100	Al_2O_3	–	–	–	–	–	–	–
	ASA	19	1.7	3	48	34	15	3

***Table* 5.** XPS data of sulfide CoMo/ASA+Al_2O_3 catalysts

Al_2O_3/ASA ratio	100/0	90/10	70/30	50/50	30/70	10/90	0/100
Mo^{4+}, %	82.8	75.9	73.4	71.3	69.5	68.9	66.8
Mo^{5+}, %	11.5	14.1	16.8	19.7	22.9	23.2	24.3
Mo^{6+}, %	5.7	10.0	9.3	9.0	7.7	7.9	8.9
Co/Mo	0.38	0.36	0.35	0.40	0.46	0.49	0.44
Co/S	0.11	0.09	0.09	0.11	0.13	0.14	0.13
Mo/S	0.30	0.28	0.35	0.45	0.4	0.44	0.37
BE S2p – 162.2 eV			BE Mo3d – 228.9 eV			BE Co2p – 779.0 eV	

intensity and high noise level. However, the Co/Mo surface ratio could be estimated from intensities of the peaks. The data show an increase in the Co/Mo ratio for the catalysts doped with ASA. The higher the ASA content, the higher the Co/Mo ratio. These data confirm the previous assumption on the improvement of promotion of MoS_2 slabs.

Catalytic activity of the catalysts was estimated in two reactions: hydrodesulfurization of thiophene and conversion of 1-hexene. *Fig*. 4 depicts the thiophene conversion obtained at 220 and 240℃. The introduction of ASA leads to a decrease in thiophene conversion from 58 to 50% at 220℃ and from 80 to 68% at 240℃. The decrease in hydrodesulfurization activity correlates with the decrease in the amount of Mo^{4+} state in XPS data and the increase in Co/Mo surface ratio. Then, it can be concluded that this reaction route is completely driven by the CoMoS phase.

The location of the CoMoS phase is also important for hydrodesulfurization activity. A comparison of the active component morphology for ASA and Al_2O_3 constituents allows us to conclude that the amount of ASA does not influence visibility, slab length and stacking number of the active component particles. Then, the dispersion of active metals is similar for the catalysts. If we increase the amount of ASA in the catalyst and do not observe changes in visibility, we can suggest that catalysts with a greater amount of ASA contain more monolayered slabs on ASA and slabs on ASA that are located parallel to the support surface. It is likely that such coordination of active component slabs on ASA is less preferable for hydrodesulfurization reaction of thiophene.

The presence of 1-hexene in the model mixture allows estimation of hydrogenation and hydroisomerization activities of the catalysts. It is known that 1-hexene transforms to n-hexane, (Z)-3-hexene, (E)-2-hexene, (E)-3-hexene and (Z)-2-hexene under the testing conditions. The amount of branched isomers was less than 0.05 wt%. The conversion of 1-hexene becomes slightly lower when ASA is introduced into the support. The remarkable effects were observed for the $HYD_{1\text{-hexene}}$ parameter, which includes

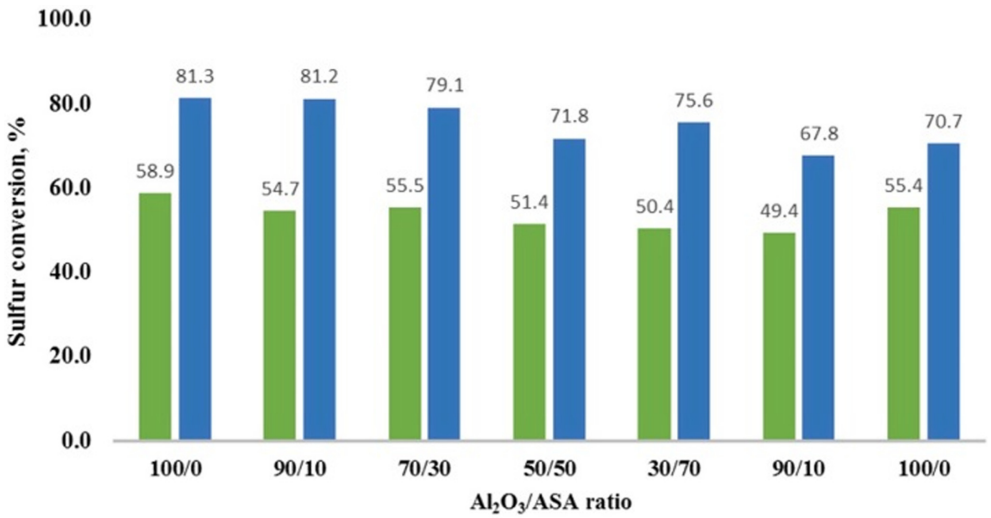

***Figure* 4.** Conversion of S per 1 ml of CoMo/Al_2O_3-ASA catalysts at 220℃ (green columns) and 240℃ (blue columns).

the conversion of 1-hexene to other isomers. The greatest decrease in the $HYD_{1\text{-hexene}}$ value is detected for the catalysts with more than 50% of ASA in the support. When ASA content achieves 50% in the support, the $HYD_{1\text{-hexene}}$ value drops by a factor of 3.

Such changes in the $HYD_{1\text{-hexene}}$ value are caused by the improvement in isomerization activity (ISO) of the catalysts. *Fig*. 5 depicts the isomerizing activity of catalysts at 220 and 240℃. The drastic change in isomerizing activity is detected for the CoMo-50/50 catalyst, especially at 240℃. Further increase in the ASA content in supports does not lead to a significant improvement in the ISO activity.

If we talk about hydrotreatment of the hydrocarbon mixture that simulates FCC gasoline, it is necessary to take into account octane numbers of the products of 1-hexene conversion because it is the most important contributor to octane number of the feedstock. Research octane number of hexene-1 is 76.4, while the products of its conversion have the following RONs: n-hexane – 24.8, 3-hexene – 94.0, and 2-hexene – 92.7. Therefore, the isomerizing products have much higher octane numbers than the initial 1-hexene. We can expect an increase in the RON number of the hydrotreated product for the case when the amount of formed isomers is significant.

RON values of the initial feedstock and hydrotreated products were calculated as the sum of RON values of the components, every of which was multiplied by the weight of the component in liquid and gas samples (Eq. 5). The RON values of the components were taken from the data in.[26] The resulting data are given in *Fig*. 6. The allowed value of the RON loss after hydrotreatment in industry is about 1.5 point. This area is shown as shaded in the chart. The RON number of the hydrotreated product grows with

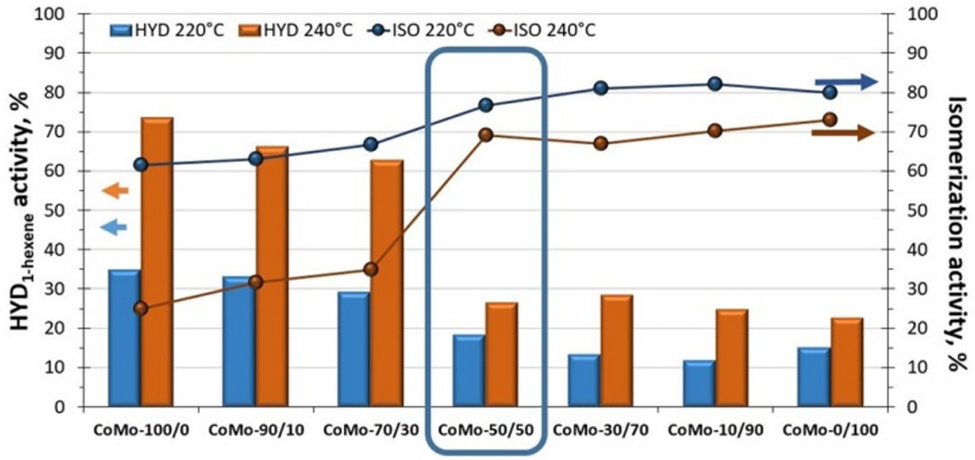

***Figure* 5.** Hydrogenation and isomerization activities of $CoMo/Al_2O_3$-ASA catalysts.

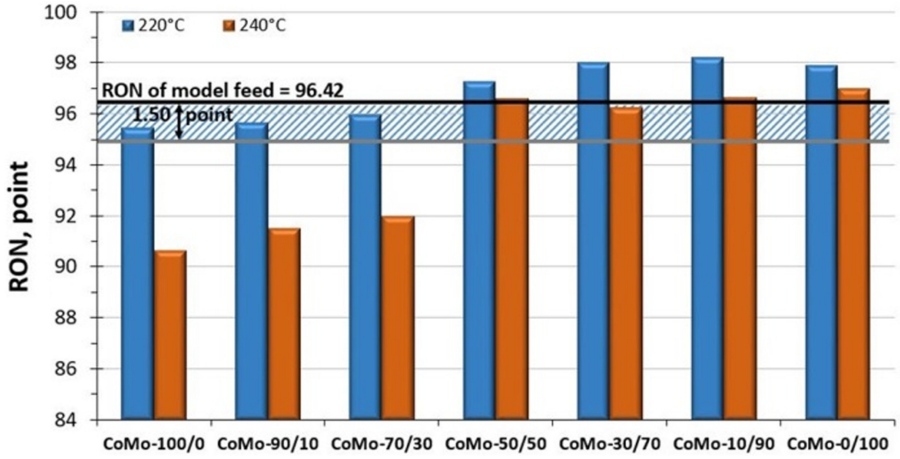

***Figure* 6.** RON of hydrotreated products and the model feedstock (the shaded area indicates the maximum allowable level of RON loss).

ASA content in the support. A significant increase in the RON value is observed for the catalyst with 50% of ASA. It was noted that the isomerizing activity of catalysts containing more than 50% of ASA was less sensitive to elevation of the process temperature. The resulting octane number of the hydrotreated product was in the range of allowed values.

The RON values are proportional to the acidity of supports and catalysts and inversely proportional to the concentration of acid sites per 1 m^2 of the surface. The RON values especially depend on the amount of medium and weak acid sites. As it was mentioned above, the strong increase in the content of medium acid sites was caused by the contribution of LAS. The increase in the content of weak acid sites could be caused by both the LAS and BAS sites.

An increase in the amount of BASs in the studied catalysts can facilitate the protonation reactions of converted molecules. Weak BASs, which are mostly present in the ASA powder and ASA-containing supports, contribute to isomerization reactions, while alkylation and cracking reactions preferentially occur with medium and strong BASs.[36] In the present work, the introduction of ASA into support influences migration of the double bond of 1-hexene followed by the preferential formation of (Z)-3-hexene, (E)-3-hexene and 2-hexenes. Migration of the double bond can be implemented by both the BASs of supports and CoMoS phase sites.

When BAS is located nearby the sulfide active component particle, an olefin is first protonated over BAS followed by the conversion at coordinately unsaturated site (CUS) of the CoMoS phase. In this case, isomerization reactions are more energetically profitable than the removal of sulfur or hydrogenation.[2,36] This can explain considerable changes in HYD and ISO activities for the samples with more than 50 wt.% of ASA (*Fig.* 7) due to the formation of weak and medium BAS in catalysts. The introduction of ASA into $CoMo/Al_2O_3$ catalysts results in an increase in the content of weak and medium LASs, which could increase the catalyst's activity in HDS of sulfur compounds.[37] Weak LASs also contribute to hydrogenation of unsaturated bonds as well as HDS of sulfur molecules due to activation of hydrogen. Small amounts of strong LASs in the studied samples can be responsible for the increased interaction between active component and support,[38–41] which has a negative influence on HDS activity.

It is interesting that some kind of a breaking point in hydrodesulfurization, hydrogenating and isomerizing activities is observed for the catalysts with 50 wt.% of ASA (*Fig.* 7). This sample demonstrates high isomerizing/low hydrogenating activity along with insignificant drop of hydrodesulfurization activity. This phenomenon can be explained by a combination of the properties of active component and support (*Fig.* 8). On the one hand, the CoMo-50/50 catalyst has a lower amount of the sulfide active phase compared to the catalyst without ASA. However, it is characterized by a higher promotion degree of the active phase than CoMo-100/0 and does not contain Co, which was separated from the CoMoS phase and interacted with the support. Therefore, the drop in hydrodesulfurization activity is not as drastic as it could be. Concerning the hydrogenating/isomerizing activity, the presence of the active phase along with the increase in the ASA con-

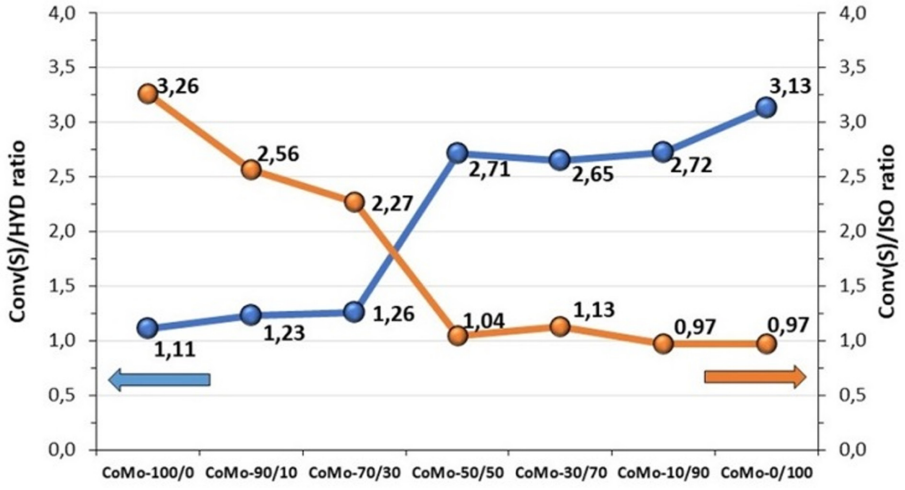

***Figure* 7.** The ratio of HDS activity to HYD and ISO ability of $CoMo/Al_2O_3$-ASA catalysts.

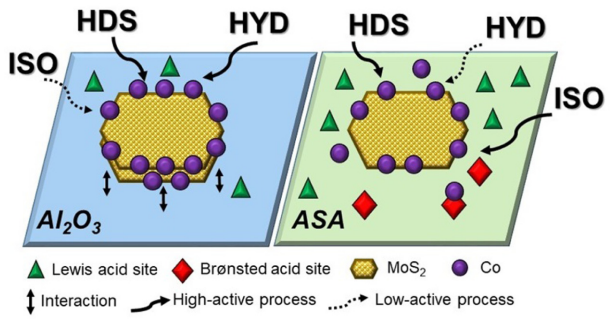

***Figure* 8.** A scheme of the processes occurring over surfaces of $CoMo/Al_2O_3$-ASA catalysts.

tent in the support will block active sites that are responsible for isomerization and hydrogenation. However, the fact is that the enhancement in the amount of isomerization active sites is more significant than of hydrogenating ones, due to the addition of 50% ASA.

Why do we point out the CoMo-50/50 catalyst instead of other catalysts with ASA content higher than 50%? The reason is that the addition of more than 50% ASA to the catalyst does not lead to considerable changes in hydrodesulfurization and hydrogenation properties, especially at high temperatures, while its performance characteristics, such as mechanical strength, become worse. The difference in mechanical strength between catalysts with 50, 70 and 90% of ASA is not very big, but the choice should be made in favor of the catalyst with the highest value of the characteristic. An increase in mechanical strength can be achieved by changing the properties of boehmite; these results will be reported in our next paper. It is known that the strength properties of the support and catalyst are significantly influenced by the morphology of alumina particles.[10] However, this topic will be covered in the next work.

CONCLUSION

The present paper studies the influence of the Al_2O_3/ASA ratio in the support on physico-chemical and catalytic properties of CoMo catalysts for FCC gasoline hydrotreating. It is shown that the addition of ASA to the support composition significantly changes textural characteristics of the supports and catalysts. There is an increase in specific surface area by more than 2 times and pore volume by more than 3 times for the supports, which also increases the corresponding characteristics for the catalysts.

The introduction of ASA into supports influences the acid characteristics of supports and then catalysts. The initial ASA powder has weak Brønsted acid sites and a large number of Lewis acid sites of weak and medium strength. The introduction of ASA into the alumina support leads to the formation of BAS and LAS, which have a noticeable effect on the structural and catalytic properties of the catalysts. First of all, there are changes in the morphology of sulfide active component particles. The catalysts with 50-100 wt.% of alumina contain active component particles preferentially on alumina. If ASA content is more than 50 wt.%, active component particles are forced to be located on the ASA compound. Then, there are changes in the interaction of active component particles and support.

The increase in the ASA content in the support composition decreases the hydrogenating activity and increases the double bond isomerization ability. The CoMoS phase location on the ASA surface and the outcome of cobalt from the active phase lead to blocking of some active sites responsible for isomerization and hydrogenation reactions. At the same time, the amount of active sites rises due to the increase in the ASA content. The introduction of more than 50 wt.% of ASA into supports allows the HDS activity of the catalysts to be maintained. However, this tendency is valid for the catalysts with the same volume. Recalculating the HDS activity to the catalysts weight shows a significant difference between the samples.

It should be noted that the most pronounced effect on hydrogenation and isomerization properties is observed at Al_2O_3/ASA = 50/50. This sample exhibits an extremely high isomerization capacity and a low hydrogenation activity. Therefore, the RON value is maintained during the hydrotreating process over this catalyst. However, the catalyst with such Al_2O_3/ASA ratio has nonoptimal bulk density and mechanical strength values. Then, additional research is required to develop a catalyst with a higher bulk crushing strength value.

Acknowledgments. This work was supported by the Ministry of Science and Higher Education of the Russian Federation within the governmental order for Boreskov Institute of Catalysis (project AAAA-A21-121011890074-4). Publication cost of this paper was supported by the Korean Chemical Society.

REFERENCES

1. Song, C.; Ma, X. *Appl. Catal. B Environ.* **2003**, *41*, 207.
2. Brunet, S.; Mey, D.; Pérot, G.; Bouchy, C.; Diehl, F. *Appl. Catal. A Gen.* **2005**, *278*, 143.

3. Toulhoat, H.; Raybaud, P. *J. Catal.* **2003**, *216*, 63.
4. Pecoraro, T. A.; Chianelli, R. R. *J. Catal.* **1981**, *67*, 430.
5. Krebs, E.; Daudin, A.; Raybaud, P. *Oil Gas Sci. Technol. – Rev. IFP Oil Gas Sci. Technol. – Rev. IFP* **2009**, *64*, 707.
6. Topsøe, H. *Appl. Catal. A Gen.* **2007**, *322*, 3.
7. Lebeau, B.; Bonne, M.; Comparot, J. D.; Rousseau, J.; Michelin, L.; Blin, J. L.; Brunet, S. *Catal. Today* **2020**, *357*, 675.
8. Delgado, A. D.; Alvarez-Contreras, L.; Beltrán, K. A.; Leyva-Porras, C.; Aguilar-Elguezabal, A. *Catal. Today* **2021**, *360*, 165.
9. Hamiye, R.; Lancelot, C.; Blanchard, P.; Toufaily, J.; Hamieh, T.; Lamonier, C. *Fuel* **2017**, *210*, 666.
10. Klimov, O. V.; Leonova, K. A.; Koryakina, G. I.; Gerasimov, E. Y.; Prosvirin, I. P.; Cherepanova, S. V.; Budukva, S. V.; Pereyma, V. Y.; Dik, P. P.; Parakhin, O. A.; Noskov, A. S. *Catal. Today* **2014**, *220*, 66.
11. Ivanova, A. S.; Litvak, G. S.; Kryukova, G. N.; Tsybulya, S. V.; Paukshtis, E. A. *Kinet. Catal.* **2000**, *41*, 122.
12. Busca, G.; ed. Jentoft, F. C. *Academic Press* **2014**, *57*, 319.
13. Nadeina, K. A.; Klimov, O. V.; Danilova, I. G.; Pereyma, V. Y.; Gerasimov, E. Y.; Prosvirin, I. P.; Noskov, A. S. *Appl. Catal. B Environ.* **2018**, *223*, 22.
14. Lei, Z.; Gao, L.; Shui, H.; Ren, S.; Wang, Z. *Energy Sources Part A-recovery Util. Environ. Eff.* **2012**, *34*, 1363.
15. Hu, E.; Yao, Z.; Zhao, L.; Wu, J.; Meng, H.; Huo, L.-W.; Li, Y. *Can. J. Chem. Eng.*
16. Kalu\vza, L. K.; Gulková, D.; Vít, Z. K.; Zdra\vzil, M. *Fuel* **2013**, *112*, 272.
17. Pérez-Martínez, D. J.; Gaigneaux, E. M.; Giraldo, S. A.; Centeno, A. *J. Mol. Catal. A Chem.* **2011**, *335*, 112.
18. Nadeina, K. A.; Klimov, O. V.; Pereima, V. Y.; Koryakina, G. I.; Danilova, I. G.; Prosvirin, I. P.; Gerasimov, E. Y.; Yegizariyan, A. M.; Noskov, A. S. *Catal. Today* **2016**, *271*, 4.
19. Pérez-Martínez, D. J.; Gaigneaux, E. M.; Giraldo, S. A. *Appl. Catal. A Gen.* **2012**, *421*, 48.
20. Ramírez, J.; Sánchez-Minero, F. *Catal. Today* DOI:10.1016/j.cattod.2007.10.103.
21. Hancsók, J.; Marsi, G.; Kasza, T.; Kalló, D. *Top. Catal.* **2011**, *54*, 1102.
22. Al-Dalama, K.; Stanislaus, A. *Energy and Fuels* DOI:10.1021/ef060125a.
23. Stolyarova, E. A.; Danilevich, V. V.; Klimov, O. V.; Gerasimov, E. Y.; Ushakov, V. A.; Chetyrin, I. A.; Lushchikova, A. E.; Saiko, A. V.; Kondrashev, D. O.; Kleimenov, A. V.; Noskov, A. S. *Catal. Today* **2019**, 1.
24. Leonova, K. A.; Klimov, O. V.; Gerasimov, E. Y.; Dik, P. P.; Pereyma, V. Y.; Budukva, S. V.; Noskov, A. S. *Adsorption* DOI:10.1007/s10450-013-9500-0.
25. Emeis, C. A. *J. Catal.* DOI:10.1006/jcat.1993.1145.
26. Ghosh, P.; Hickey, K. J.; Jaffe, S. B. *Ind. Eng. Chem. Res.* **2006**, *45*, 337.
27. Engelhardt, G.; Michel, D. *High Resolution Solid State NMR of Silicates and Zeolites*; Chichester, New York, John Wiley: 1987.
28. Krivoruchko, O. P.; Gavrilov, V. Y.; Molina, I. Y.; Larina, T. V. *Kinet. Catal.* DOI:10.1134/S0023158408020171.
29. Sánchez-Minero, F.; Ramírez, J.; Gutiérrez-Alejandre, A.; Fernández-Vargas, C.; Torres-Mancera, P.; Cuevas-Garcia, R. *Catal. Today* **2008**, *133*, 267.
30. Koizumi, N.; Hamabe, Y.; Yoshida, S.; Yamada, M. *Appl. Catal. A Gen.* **2010**, *383*, 79.
31. de Jong, A. M.; de Beer, V. H. J. (San); van Veen, J. A. R.; Niemantsverdriet, J. W. (Hans). *J. Phys. Chem.* **1996**, *100*, 17722.
32. Sanders, A. F. H.; de Jong, A. M.; de Beer, V. H. J.; van Veen, J. A. R.; Niemantsverdriet, J. W. *Appl. Surf. Sci.* **1999**, *144*, 380.
33. Swami, S. K.; Chaturvedi, N.; Kumar, A.; Kapoor, R.; Dutta, V.; Frey, J.; Moehl, T.; Grätzel, M.; Mathew, S.; Nazeeruddin, M. K. *J. Power Sources* DOI:10.1016/j.jpowsour.2014.11.003.
34. Frizi, N.; Blanchard, P.; Payen, E.; Baranek, P.; Lancelot, C.; Rebeilleau, M.; Dupuy, C.; Dath, J. P. *Catal. Today* DOI:10.1016/j.cattod.2007.10.008.
35. Gandubert, A. D.; Krebs, E.; Legens, C.; Costa, D.; Guillaume, D.; Raybaud, P. *Catal. Today* DOI:10.1016/j.cattod.2007.06.041.
36. Corma, A. *Chem. Rev.* DOI:10.1021/cr00035a006.
37. Eijsbouts, S. In *Synthesis of Solid Catalysts* Wiley-VCH Verlag GmbH & Co. KGaA: Weinheim, Germany 2009; pp. 301–328.
38. Tahmasebi, K.; Paydar, M. H. *Mater. Chem. Phys.* DOI:10.1016/j.matchemphys.2007.11.009.
39. Cao, J.; Xia, J.; Zhang, Y.; Liu, X.; Bai, L.; Xu, J.; Yang, C. A.; Zheng, S.; Yang, T.; Tang, K.; Zhang, C.; Zhou, C. *Fuel* **2021**, *289*, 119843.
40. Lauritsen, J. V.; Kibsgaard, J.; Olesen, G. H.; Moses, P. G.; Hinnemann, B.; Helveg, S.; Nørskov, J. K.; Clausen, B. S.; Topsøe, H.; Lægsgaard, E. **2007**, *249*, 220.
41. Bouwens, S. M. A. M.; Van Zon, F. B. M.; Vandijk, M. P.; Van der Kraan, A. M.; Debeer, V. H. J.; Van Veen, J. A. R.; Koningsberger, D. C. *J. Catal.* DOI:10.1006/jcat.1994.1076.